Astrophys Space Sci (2013) 343:75–82
DOI 10.1007/s10509-012-1220-5

ORIGINAL ARTICLE

Resonant orbits in the vicinity of asteroid 216 Kleopatra

Yang Yu · Hexi Baoyin

Received: 25 May 2012 / Accepted: 13 August 2012 / Published online: 12 September 2012

Abstract This investigation examines the resonant orbits in the vicinity of asteroid 216 Kleopatra using a precise gravitational model, with emphasis on their crucial role in determining the global orbital behaviors. Three-dimensional Monte Carlo simulations of test particle trajectories are launched to find the condition and probability distribution of resonance. It is revealed the resonant orbits are rich and concentrated in the near-field regime, which provides a short-term mechanism to clear the vicinal ejecta away from the asteroid. The unstable boundary predicted in our calculations is consistent with the observed mutual orbits of satellites S/2008 (216) 1 and S/2008 (216) 2. The probability distribution of resonance is considered as an indicator of the stability of vicinal orbits, and the results are identical to the previous analysis by Scheeres et al. (Icarus 121:67, 1996) for the stability of retrograde orbits around asteroid 4769 Castalia.

Keywords Celestial mechanics—methods · Numerical—planets and satellites · Dynamical evolution and stability—minor planets · Asteroids · Individual · 216 Kleopatra

1 Introduction

Motion close to an asteroid usually represents high risk for the spacecraft during in-situ exploration, both due to inadequate prior observations and the complexity of the dynamics (Cheng 2002). Since every asteroid has a unique size, shape, density and rotation state, careful study is required to precisely estimate these quantities before close-proximity missions (e.g. the first landing of JAXA's Hayabusa spacecraft on 25143 Itokawa) (Scheeres et al. 2006; Fujiwara et al. 2006). Essentially, the risk of close orbital missions comes from the complicated gravitational environment primarily induced from the rotating irregularly shaped asteroid, which might lead to unstable and chaotic orbits and make the final fates of natural objects and spacecraft unpredictable (Scheeres et al. 1996).

A resonance effect was found near asteroid 4769 Castalia arising from the commensuration between the asteroid rotation rate and the particle true anomaly rate at periapsis by Scheeres et al. (1996), based on a second-degree and -order gravitational field model. This effect is regarded as playing an important role in the complex dynamical environment in the vicinity of asteroids for it provides a short-term mechanism (of order the spin period) to eject orbiting objects into hyperbolic trajectories, or conversely to capture ejectas into temporarily cycling orbits. Particularly, recent investigations showed the resonance represents a realistic threat to NASA's DAWN mission (Russell et al. 2007), that is, the probe might be locked into a resonance orbit from which its thrusters cannot escape, during the rendezvous with Vesta. This gravity trap bound was found near the 1:1 spin-orbit resonance and located in a polar orbit of attitude about 520–580 km by Tricarico and Sykes (2010).

On the other hand, various groups have demonstrated numerically that several mechanisms can lead to the disruption of asteroids consisting of loosely consolidated material (Richardson et al. 1998; Durda et al. 2004; Walsh et al. 2008, 2012), which might create plenty of ejectas in the vicinity of the primary asteroids. The trajectories of these ejectas were grouped into five classes by Scheeres et al. (2002), and their final states were shown to depend dramatically on the initial conditions. These close orbital behaviors could

Y. Yu · H. Baoyin (✉)
School of Aerospace, Tsinghua University, 100084 Beijing, China
e-mail: baoyin@tsinghua.edu.cn

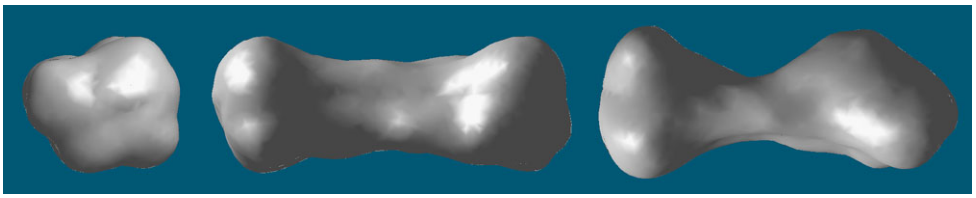

Fig. 1 The inversion image of 216 Kleopatra based on radar observations (Neese 2004). Side view (*left*), face view (*center*) and top view (*right*). The topography is highly elongated in a single direction and surprisingly bulges at both ends

have profound effects on surface geological processes and the formation of vicinal satellites. Most observed satellites of main-belt asteroids with primary diameters smaller than about 20 km (Johnston 2012) possess orbital semi-major axes of $2 \sim 5$ times the maximum dimension of the primary (Richardson and Walsh 2006; Marchis et al. 2008a, 2008b). The resonance effect might play an important role in the elimination of vicinal ejecta during the short term, which will help in the understanding of the regularity of binary systems' mutual orbits.

In this study, we take a detailed look at the resonant orbits in the vicinity of asteroid 216 Kleopatra. The detailed gravitational model is used to approximate the irregular field near the asteroid, instead of the homogenous simple geometry or truncation of harmonics. Global orbital behaviors in the near-field regime are examined over wide ranges of parameters to clarify the universality of resonant orbits, and further, to find the resonant conditions and determine the probability distribution of resonance quantificationally. The instantaneous orbital energy is taken as the discriminator of this resonance effect; the distribution of gravitational power is demonstrated using the detailed gravity model. Then three-dimensional Monte Carlo simulations of trajectories near the equatorial plane are carried out over a wide representative parameter space. The results show a very regular distribution of the resonance conditions and reveal significant connections between the Jacobi constant and the resonance effects. It is confirmed that natural ejecting orbits exist widely in the vicinity of Kleopatra to clear ejecta away.

2 (216) Kleopatra: detailed gravity model

Reconstruction of the actual dynamical environments about asteroids has been enabled thanks to shape determinations through radar observations and in some case in-situ visits (Ostro et al. 2002; Robert et al. 2002). The polyhedral method developed by Werner and Scheeres (1997) has been used widely to precisely evaluate the gravitational field around specific asteroids such as 4179 Toutatis, 433 Eros and 25143 Itokawa (Scheeres et al. 1998, 2006; Yeomans et al. 2000).

Main-belt asteroid 216 Kleopatra is of particular interest: the mysterious dog-bone shape generates a dominant second-degree and -order gravitational field, and a fast rotation rate suggests a high probability of resonance near its surface (Ostro et al. 2000; Hu and Scheeres 2004); moreover, Kleopatra is a triple asteroid with two small satellites (S/2008 (216) 1 and S/2008 (216) 2) observed in 2008 (Marchis et al. 2008c), which makes it a natural laboratory to test the performance of the dynamical studies.

A detailed model of Kleopatra's gravitational field can be obtained from the radar-derived shape model (Ostro et al. 2000). Figure 1 illustrates the dog-bone shape of asteroid 216 Kleopatra. Supposing this polyhedral model is homogeneous, the mass-distribution parameter can be calculated at $\sim$0.99, which is defined as a function of the body principal moments of inertia (Yu and Baoyin 2012), and indicates large coefficients of second degree and order that contributes to the resonance as a dominant factor.

2048 vertices and 4096 faces are included in this polyhedral model (Neese 2004) with the rotation period $\sim$5.385 hours and total mass estimated to be $4.64 \pm 0.02 \times 10^{18}$ kg (Descamps et al. 2011). Since the motion in the near-field regime is limited to a region of 10 times the maximum dimension of the asteroid, we take the Hill sphere $\sim 2.89 \times 10^4$ km to be the limit of major perturbation from solar gravity (Hamilton and Burns 1992), and all gravitational perturbations from all the remaining celestial bodies are neglected. Two coordinate systems are used throughout this paper. The first is an inertial frame CXYZ with the origin located at the mass center; the second is a body-fixed frame Cxyz with the three axes corresponding to the principal axes of the smallest, intermediate, and largest moments of inertia, respectively.

3 General orbit dynamics and energy equations

Scheeres et al. (1998) presented the complete form of the equations of motion (1) for a small particle in the body-fixed frame based on the polyhedral gravitational model. By introducing the effective potential, which is the combination of the centrifugal and gravitational potentials, the equations of motion are formulated to Hamiltonian form (Scheeres et al. 1998).

$$\ddot{\mathbf{r}} + 2\boldsymbol{\omega} \times \dot{\mathbf{r}} + \boldsymbol{\omega} \times (\boldsymbol{\omega} \times \mathbf{r}) = -\nabla U, \tag{1}$$

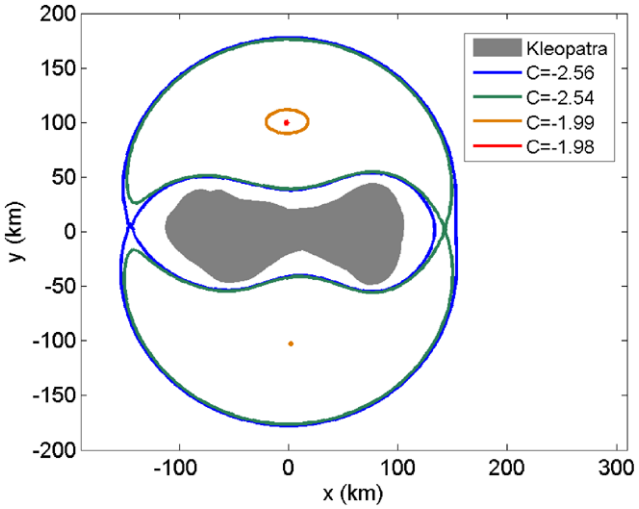

Fig. 2 The zero-velocity surfaces at the critical values of the five categories stated in the main text, demonstrated in the equatorial plane ($z = 0$); unit: 10^{-3} km^2/s^2

or

$$\ddot{\mathbf{r}} + 2\boldsymbol{\omega} \times \dot{\mathbf{r}} = -\nabla V. \tag{2}$$

Where $\mathbf{r}$ is the radius vector of the particle, $\boldsymbol{\omega}$ is the angular velocity vector of Kleopatra (assumed to be a constant vector parallel to the primary rotation axis), U is the gravitational potential and $V = -\|\boldsymbol{\omega} \times \mathbf{r}\|^2/2 + U$ is the effective potential. The dissipationless form of Eq. (2) indicates the absence of asymptotic behaviors of system, so the Hamiltonian function (3) is a generalized energy integral, called the Jacobi constant.

$$H(\mathbf{r}, \dot{\mathbf{r}}) = \frac{1}{2}\dot{\mathbf{r}} \cdot \mathbf{r} + V(\mathbf{r}) = C. \tag{3}$$

The Jacobi constant can be used to discriminate the allowable and forbidden regions around Kleopatra, which are separated by the zero-velocity surfaces, as demonstrated in Yu and Baoyin (2012). Supposing the test particle is of unit mass, all the energy quantities in this paper are assumed to be specific energies. The zero-velocity surfaces are inherently related with the orbital structures in the region close to these surfaces (Szebehely 1967), and provide a natural categorization of the vicinal orbital motion to immediately determine if the orbit will impact or escape from the asteroid eventually. As illustrated in Fig. 2, to take a view of the equatorial plane, five categories of motion are obtained based on the topology of these curves: I. The equatorial plane is globally accessible (-1.98×10^{-3} km^2/s$^2 < C$); II. An isolated island is forbidden on one side (-1.99×10^{-3} km^2/s$^2 < C < -1.98 \times 10^{-3}$ km^2/s^2); III. Two branches are forbidden on both flanks (-2.54×10^{-3} km^2/s$^2 < C < -1.99 \times 10^{-3}$ km^2/s^2); IV. Connected branches make a narrow neck to permit the inside initialized orbits to escape (-2.56×10^{-3} km^2/s$^2 < C < -2.54 \times 10^{-3}$ km^2/s^2); V. Closed forbidden region separates the orbits inside and outside ($C < -2.56 \times 10^{-3}$ km^2/s^2).

More results on general dynamics in the vicinity of asteroids can be achieved from the studies of other elongated shaped asteroids. Scheeres et al. (1996) examined the orbits close to asteroid 4769 Castalia with a detailed polyhedral model, revealing the existence of unstable synchronous orbits, mostly stable retrograde orbits and periodic orbit families around this asteroid. Further investigations were published later (Scheeres et al. 2000; San-Juan et al. 2004) on the periodic orbits and their stability around asteroid 433 Eros (Maria et al. 2000), in which the minimum stable radii were determined both for the prograde and retrograde circular orbits according to the resonance conditions.

Generally, the dynamical features stated above are derived from the complex instability of orbital structures in the vicinity of asteroids, and are essentially reflected in the variations of mechanical energy. Scheeres et al. (1996) demonstrated the Keplerian energy effects based on the second-degree and -order gravitational field. Since the magnitude of the orbital energy has been found to be a distinguishing factor for determining the final outcomes of orbits (Scheeres et al. 2002), we examine the energy features of orbits in the near-field regime, including those caught in resonance and that end with impact or escape.

Recall the definition of orbital energy (4), which is not conserved due to exchange from Kleopatra's rotational kinetic energy (any effect on the asteroid's rotation is tiny and ignorable).

$$E = U(\mathbf{r}) + \frac{1}{2}\|\boldsymbol{\omega} \times \mathbf{r} + \dot{\mathbf{r}}\|^2. \tag{4}$$

Combining with the conserved quantity Eq. (3) yields

$$E = C + \boldsymbol{\omega} \cdot \mathbf{L}, \tag{5}$$

where $\mathbf{L} = \mathbf{r} \times (\boldsymbol{\omega} \times \mathbf{r} + \dot{\mathbf{r}})$ is the specific orbital angular momentum, with the time derivative determined by (6). In Eq. (5), the orbital energy and angular momentum are relative to the inertial frame and represented with quantities of the body-fixed frame. Then the general form of gravity power is given by Eq. (7), which is only position dependent. Namely, a spatial scalar field in the body-fixed frame is fully determined by the geometry of the gravitational field, which retains a stationary regime that governs the energy exchanges for arbitrary motion inside.

$$\frac{d}{dt}\mathbf{L} = -\mathbf{r} \times \nabla U(\mathbf{r}), \tag{6}$$

$$p(\mathbf{r}) = \frac{d}{dt}E = -(\boldsymbol{\omega} \times \mathbf{r})\nabla U(\mathbf{r}). \tag{7}$$

Figure 3 illustrates this power field in the equatorial plane ($z = 0$), that is, the rotational axis is perpendicular to the plane. The value of gravitational power distributes approximately symmetrically in four quadrants: I. $x > 0$, $y > 0$;

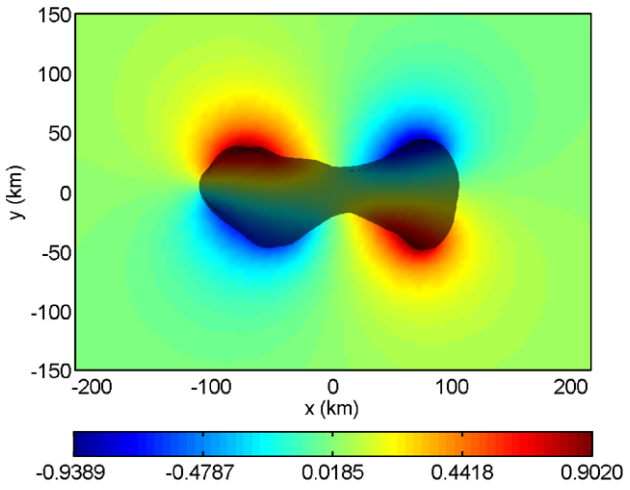

Fig. 3 The colormap of gravity power in the equatorial plane; the *shadowed area* sketches the shape of Kleopatra, and the *color* indicates the energy power magnitude at each point (unit: m^2/s^3)

II. $x < 0$, $y > 0$; III. $x < 0$, $y < 0$; IV. $x > 0$, $y < 0$. Generally, the power is positive in quadrants II and IV and negative in quadrants I and III, and decreases rapidly with distance from the asteroid (e.g., over 150 km away from the origin, the power is everywhere below 10 % of the maximum value). These conclusions are largely consistent with the analysis based on the second-degree and -order gravitational model of prolate body (Scheeres et al. 1996), indicating this model plays as a dominant role in the motion around prolate asteroids. Besides, Fig. 3 indicates that the extreme power values are reached at locations where the terrain significantly rises up. It suggests more possibilities for the surface particles in quadrants I and III to be ejected from the asteroid than those of the quadrants II and IV, which has implications for the evolution of regolith, which is related both with the ejecta dynamics and the geography of asteroid (Scheeres et al. 2002).

Equation (5) also delimits the orbital energy in the body-fixed frame; and by using Eq. (3), we obtain

$$E = C + \|\boldsymbol{\omega} \times \mathbf{r}\|^2 + \varepsilon \cdot \|\boldsymbol{\omega} \times \mathbf{r}\| \cdot \sqrt{2\big(C - V(\mathbf{r})\big)}. \tag{8}$$

In which the last item indicates the inner product of the convected velocity vector $\boldsymbol{\omega} \times \mathbf{r}$ and relative velocity vector $\dot{\mathbf{r}}$, and $\varepsilon \in [-1, 1]$ indicates the cosine of included angle between these two vectors. Equation (8) shows that the magnitude of instantaneous orbital energy depends on the Jacobi constant, which provides a direct criterion for orbits escaping from the neighborhood of asteroids. Since the motion close to zero-velocity surfaces is usually sensitive while the motion distant from the asteroid is more robust, the third term of Eq. (8) shows a basic reason: the included angle between the convected and relative velocities suffers a sharp variation close to the zero-velocity surfaces which resulted in the sudden energy increment. Besides, the range of orbital energy can be determined in the third term of Eq. (8): it is about zero close to the zero-velocity surface and grows quadratically with distance from the asteroid.

4 Resonance: condition and probability

The possibility of natural ejecting and capturing orbits was first mentioned by Miller in 1993 (Scheeres et al. 1996). Then it was defined as resonance effect in a second-degree truncation of the gravitational field and concluded that this effect is driven primarily by the interaction between the orbital motion, the C_{22} gravity coefficient and the asteroid rotation rate (Scheeres et al. 1996). However, more abundant resonance effects might be generated by the high-order terms of the gravitational field, which would suggest more possibilities to clear the surrounding ejecta away. In this section, the resonance effect is examined using a precise gravitational field model. An explicit criterion for resonance likely does not exist for there is no analytical solution to the system (2); instead, the instantaneous orbital energy is regarded as an indicator of resonance effects due to its significant links both to the gravitational field's geometry and to the orbital patterns (e.g., ellipse, hyperbola and parabola). In most instances, obvious resonances are detected when the orbital energy shows an abrupt change, which is primarily caused by a reversal in relative velocity in a small region, as the magnitude of ε varies in Eq. (8). We can delineate several distinct types of resonance effects due to the orbital patterns before and after this interaction. Figure 4 illustrates three typical classes of resonance for which the orbital energy increases (those for which the energy decreases exist correspondingly): class I is a cycling orbit with the instantaneous eccentricity increasing sharply; class II is an orbit converted from cycling to escaping; class III is a hyperbolic orbit with the escaping velocity magnitude increasing sharply during the interaction. The adaptive step size Runge-Kutta method (order of 7–8) was adopted for the numerical integration, due to the consideration of the convergence and computational efficiency.

Obviously, the magnitude of orbital energy corresponds to the final fates of the orbits: positive values indicate an escaping motion; negative values indicate temporary cycling motion and insufficient energy may lead to an impact on the asteroid. It provides the criterion for orbital pattern conversion in the inertial frame, e.g., the ejected orbit, or a hyperbolic trajectory captured into an orbit circling around the asteroid.

Obvious energy exchanges are primarily obtained in the near-field regime; numerous simulations of 216 Kleopatra reveal that two dominant mechanisms exist in these motions. The first is the 1:1 resonance induced by the unstable manifolds of four equilibria around Kleopatra, which lead to

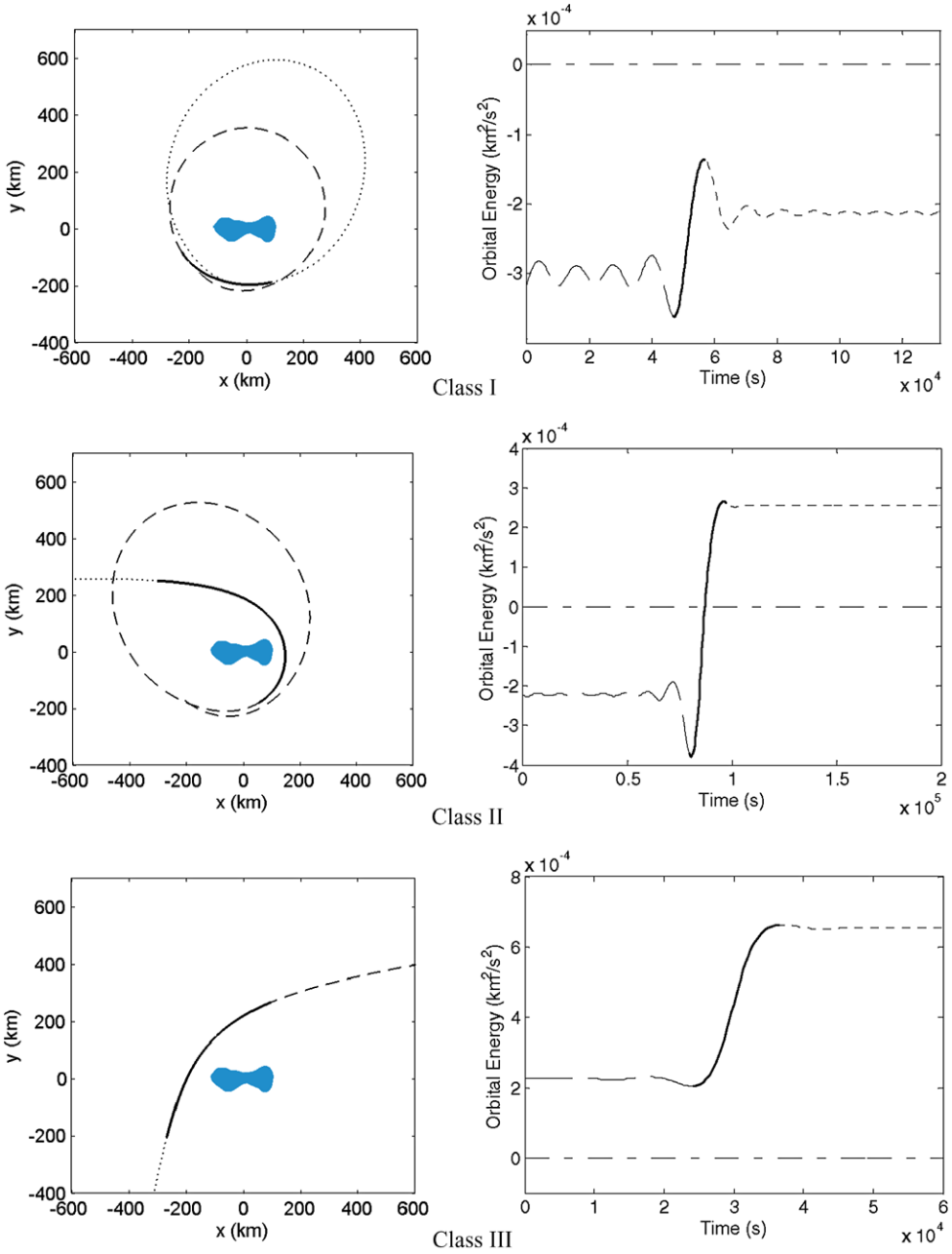

Fig. 4 The typical classes of resonance with positive energy increments, including the three segments of orbits in the inertial frame and the instantaneous orbital energy varying with time. The *dashed line*, *solid line* and *dotted line* indicate the three segments of orbits before, during and after the interaction. And the *dash-dotted line* indicates zero energy

the complex instability of the adjacent trajectories and determine the pattern of trajectories departing from corresponding equilibria (Yu and Baoyin 2012). The second is more pervasive among the trajectories in the vicinity of Kleopatra; this biased temporary synchronism presents as a sharp reversal in relative velocity in the neighborhood of zero-velocity surfaces. Essentially, this temporary synchronization results from the trajectory sticking close to the zero-velocity surface, and indicates a monotonous change of the instantaneous energy. The final outcomes of these motions fall into classes I–III in Fig. 4 (taking the cases with increasing energy for instance).

4.1 Conditions of resonance effects

In this section we sketch the distribution of the second type of resonance, i.e. the temporary synchronism stated above, through ergodic searching of the orbits close to Kleopatra in the equatorial plane. To understand further the role of resonance in the proximal orbital behavior, the dependence of resonance conditions on the Jacobi constant is investigated. Remarkable features are identified for a wide range of Jacobi constant value.

Due to the general symmetry of the dynamical environment in the four quadrants of Fig. 3, our numerical simulations are restricted to trajectories initiated in quadrant II as a

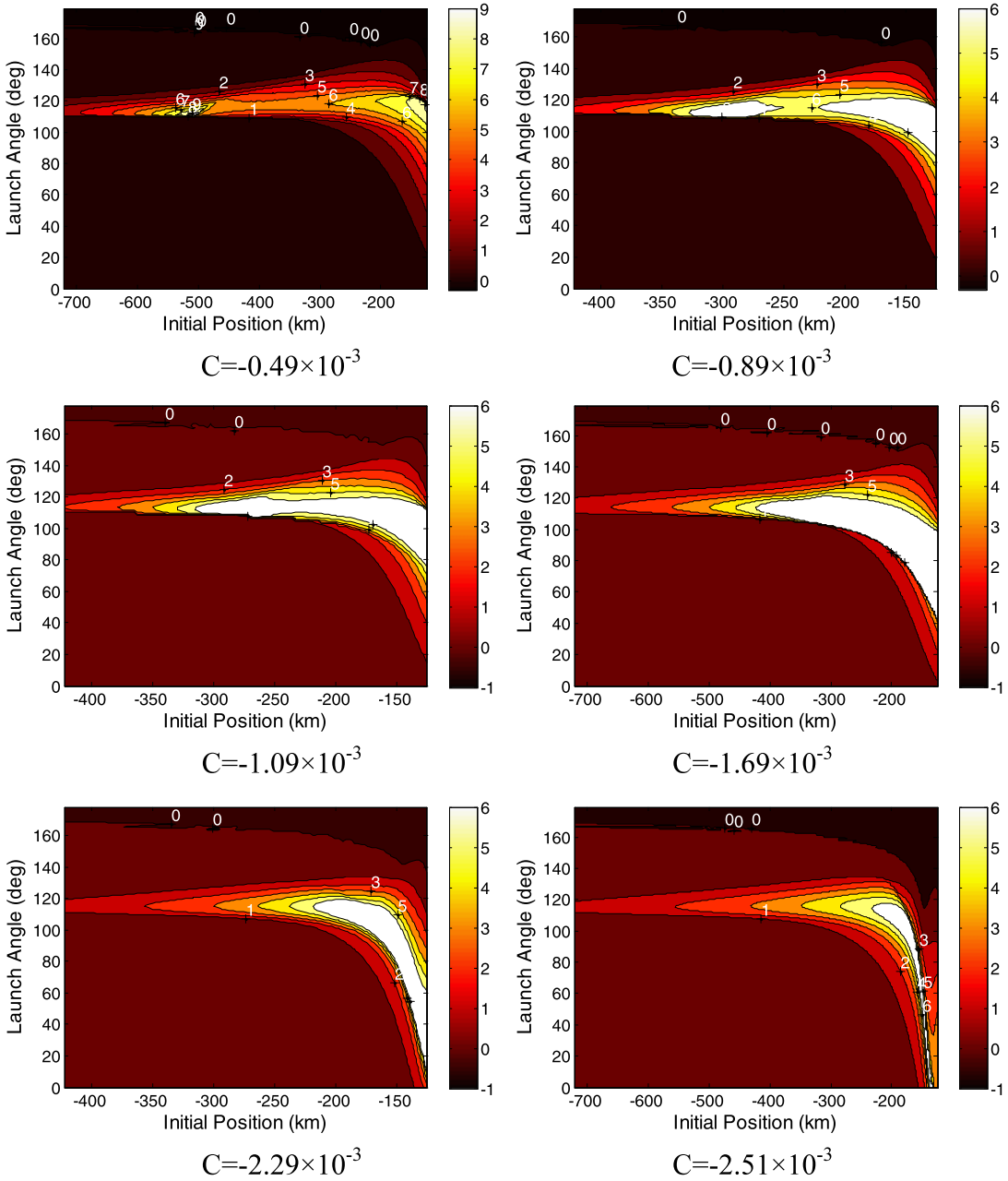

Fig. 5 The distribution of energy increment of the orbits located in quadrant II from Monte Carlo simulations for six values of the Jacobi constant; units: 10^{-4} km^2/s^2. The results are shown as a function of the initial position away from the origin along the $-x$ axis and the launch angle from the $-x$ direction. In these simulations, 300,000 test particles were integrated

representive sample. The initial position of the test particle is settled at the $-x$ axis and the value of Jacobi constant is assigned as a governing parameter, thus the initial position from the origin and launch angle from the $-x$ direction are chosen as two coordinates to uniquely describe the initial orbits in the equatorial plane, which enables a global searching for the resonant solutions. The test particles are generated as follows: the initial locations are randomly on the $-x$ axis in the range $(-7.19, -1.25) \times 10^2$ km. The magnitudes of velocities are chosen in accordance with the value of the Jacobi constant, in the range $(-2.55, 0.49) \times 10^{-3}$ km^2/s^2. And the directions of velocities are randomly chosen between 0° and 180°, that is, the test trajectories are all located in quadrant II.

Figure 5 shows the distribution of orbital energy increment of these orbits located in quadrant II for 6 different Jacobi constants, derived from Monte Carlo simulations that survive a cut-off condition of colliding with the asteroid or

departing from quadrant II. The results of Fig. 3 show all the trajectories started in quadrant II will leave this quadrant eventually, so no limitation of integration time was set in these simulations. These six contour maps show representative results for the simulations at different values of Jacobi constant for a wide range. A clear trend with the increasing initial position and launch angle is found, which appears as a bending, rising ridge with the corner near (−250 km, 120°). Two main features are apparent as the Jacobi constant increases: one is a primary region of resonance (the highlighted area close to the asteroid) close to the asteroid with a wide range of launch angle ($C < -1.98 \times 10^{-3}$ km^2/s^2), corresponding to the dense trajectories of temporary synchronization. The other is a secondary region of resonance (the isolated highlighted area in the middle), which is separated from the primary region ($C > -1.79 \times 10^{-3}$ km^2/s^2) and gets further apart as C increases, which are confirmed to be mostly hyperbolic orbits of class III.

More specifically, an invariant trend for the distribution of resonant orbits is found for a wide range of Jacobi constant, which is at about 115° launch angle when the initial position is far from the asteroid. The same asymptotic distribution is found with a simplified gravitational model of second degree and order employed, showing that these gravitational harmonics play a leading role in the resonance far from the asteroid; as the initial position approaches the asteroid, this distribution shows a separation between the simplified model and detailed model, indicating that higher-order gravitational harmonics contribute a lot to the orbital behavior in the near vicinity of Kleopatra.

Taking the energy increment during one quadrant as an appropriate criterion for the orbits suffering resonance, the locations of resonance show quite a regular distribution: significant increments concentrate on the bending narrow band with two main resonant locations inside, away from which the magnitudes rapidly decay to zero; this distribution are markedly different in the near- and far-field regimes, which are sensitive to the Jacobi constant in the near vicinity of Kleopatra (above −300 km) but show less dependence on this constant at further distances (below −300 km).

Figure 6 illustrates the extreme values of orbital energy increments as a function of Jacobi constant, which are located around the primary and secondary resonances shown in Fig. 5. Detailed examinations of these orbital patterns show the following points: most orbits at the primary resonance fall into class I when -2.17×10^{-3} km^2/s^2 $< C <$ 0.11×10^{-3} km^2/s^2; the secondary resonance at $-1.79 \times$ 10^{-3} km^2/s^2 $< C < -0.19 \times 10^{-3}$ km^2/s^2 gains larger energy increments than the primary, and most orbits in these cases fall into class III; generally, the orbits of primary resonance has complicated components of all three classes I–III.

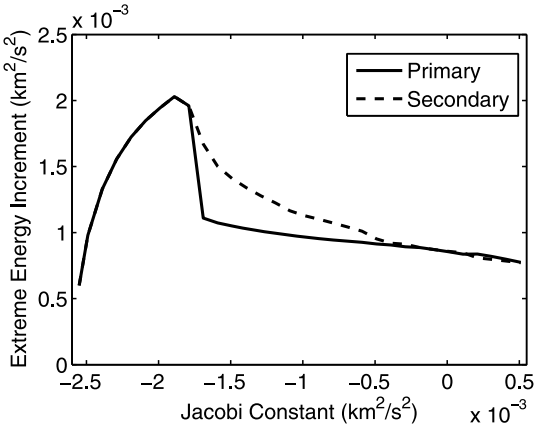

Fig. 6 The extreme value of the primary and secondary resonances for different Jacobi constants, from -2.55×10^{-3} to 0.51×10^{-3} km^2/s^2

4.2 Probability distribution of ejecting orbits

Generally, the outcomes of orbits initially circling the asteroid include long-term stable orbits, escape from the gravity of the asteroid and impact on the asteroid after an extended period of time. Special attention is paid to the second case (natural ejecting orbits) in this study, which might be induced from strong short-term resonance effects, as demonstrated in class II of Fig. 4. Since it provides a quick mechanism to perturb the near-field material away from it, this section examines its universality by simulating for longer time and find the fates of test particles. The time variation of instantaneous orbital energy is checked with the criterion of crossing zero from negative to positive (class II). We examine all the orbits passing through quadrant II in wide parameter space to identify these characteristic orbits, and further to determine the probability distribution of the occurrence of ejecting orbits. The normalized probability is defined as the proportion of the launch angles range of ejecting in the total range of 180 degrees.

Figure 7 illustrates the normalized probability distribution of the ejected orbits from Monte Carlo simulations, which is composed of all those suffering orbital energy exchanges from negative to positive with a strong resonance (natural ejecting orbits switched in quadrant II). The distribution is shown as a function of the Jacobi constant from -2.55×10^{-3} km^2/s^2 to 5.31×10^{-3} km^2/s^2 and the initial position from −421 km to −125 km. Several points are reflected in this figure. The natural ejecting orbits are numerous in the vicinity of Kleopatra, and the extreme value of the probability is ∼0.073 at $-1.92 \times$ 10^{-3} km^2/s^2 and −202.2 km. This could be a primary force to clear the vicinal circling material away from this asteroid. As demonstrated, concentrated ejecting orbits are located largely above −320 km, and below this value, this interaction becomes very weak (probability ∼0.0). This is fully consistent with the observed semi-major axis of the

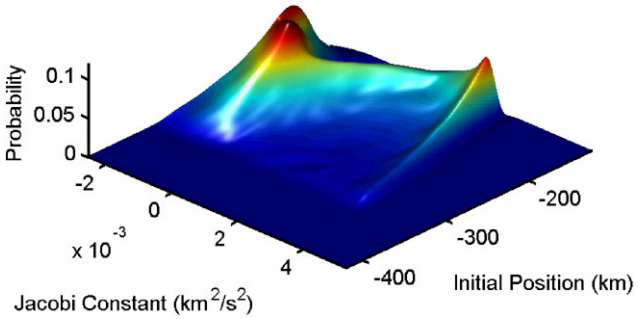

Fig. 7 The normalized probability distribution of natural ejecting orbits which present positive crossing over the critical energy zero in Monte Carlo simulations. The results are shown as a function of the initial position and Jacobi constant. 250,000 test particles were generated

two satellites, which are ∼454 km and ∼678 km (Descamps et al. 2011). The probability of ejecting orbits also depends on the Jacobi constant: around -1.92×10^{-3} km^2/s^2 and 2.81×10^{-3} km^2/s^2, the ejecting orbits are particularly abundant through a wide range of initial position. It is notable that natural ejecting orbits will disappear when $C > 3.41 \times 10^{-3}$ km^2/s^2, in which case all initially circling orbits are retrograde; and when $C < -1.39 \times 10^{-3}$ km^2/s^2, no circling orbits present retrograde. This result could largely explain the special stability of retrograde orbits, that the large relative angular motion diminishes the resonance effect (Scheeres et al. 2000).

5 Conclusions

This paper investigated the resonant orbits in the neighborhood of asteroid 216 Kleopatra using a precise model of its gravitational field, with the aim of developing a basic understanding of the effect of resonances in the vicinal orbital motion. The increment of instantaneous orbital energy is regarded as the criterion for the determination of resonant orbits, leading to three distinct classes of these orbits. The results from Monte Carlo simulations show that resonant orbits are abundant in the near-field regime, and the distribution is qualitatively consistent with that under 2nd-degree and—order model, but strongly influenced by high-order gravitational harmonics at some locations. In particular, natural ejecting orbits are shown to be an important short-term mechanism to clear the ejectas in the vicinity of Kleopatra away; the boundary predicted numerically is consistent with the observed mutual orbits of its satellites S/2008 (216) 1 and S/2008 (216) 2. Notable connections between the Jacobi constant and the distribution of resonant orbits are considered in the global orbital behavior around Kleopatra, which derive from temporary synchronism close to the geometry of the zero-velocity surface. The Jacobi constant range where these orbits are densely distributed indicates unstable vicinal motion set; and the special stability of retrograde orbits close to the asteroid is confirmed due to the low probability when Jacobi constant is very large.

Acknowledgements This work was supported by the National Basic Research Program of China (973 Program, 2012CB720000) and the National Natural Science Foundation of China (No. 11072122).

References

Cheng, A.F.: In: William, F., et al. (eds.) Asteroids III, p. 351. University of Arizona Press, Tucson (2002)
Descamps, P., Marchis, F., Berthier, J., et al.: Icarus **211**, 1022 (2011)
Durda, D.D., Bottke, W.F. Jr., Enke B.L., et al.: Icarus **167**, 382 (2004)
Fujiwara, A., Kawaguchi, J., Yeomans, D.K., et al.: Science **312**, 1330 (2006)
Hamilton, D.P., Burns, J.A.: Icarus **96**, 43 (1992)
Hu, W., Scheeres, D.J.: Planet. Space Sci. **52**, 8 (2004)
Johnston, W.R.: Binary minor planets V5.0. EAR A COMPIL 5 BINMP V5.0, NASA Planetary Data System (2012)
Marchis, F., Descamps, P., Baek, M., et al.: Icarus **196**, 97 (2008a)
Marchis, F., Descamps, P., Berthier, J., et al.: Icarus **195**, 295 (2008b)
Marchis, F., Descamps, P., Berthier, J., Emery, J.P.: IAU Circ. **8980**, 1 (2008c)
Maria, T.Z., David, E.S., Cheng, A.F., et al.: Science **2101**, 2097 (2000)
Neese, C. (ed.): Small body radar shape models V2.0. NASA Planetary Data System (2004)
Ostro, S.J., Hudson, R.S., Nolan, M.C., et al.: Science **288**, 836 (2000)
Ostro, S.J., Hudson, R.S., Benner, L.A.M., et al.: In: William, F., et al. (eds.) Asteroids III, p. 151. University of Arizona Press, Tucson (2002)
Richardson, D.C., Walsh, K.J.: Annu. Rev. Earth Planet. Sci. **34**, 47 (2006)
Richardson, D.C., Bottke, W.F. Jr., Love, S.G.: Icarus **134**, 47 (1998)
Robert, F., Jun'ichiro, K., Christopher, T.R., et al.: In: William, F., et al. (eds.) Asteroids III, p. 367. University of Arizona Press, Tucson (2002)
Russell, C.T., Capaccioni, F., Coradini, A., et al.: Earth Moon Planets **101**, 1 (2007)
San-Juan, J.F., Abad, A., Lara, M., Scheeres, D.J.: J. Guid. Control Dyn. **27**, 2 (2004)
Scheeres, D.J., Ostro, S.J., Hudson, R.S., Werner, R.A.: Icarus **121**, 67 (1996)
Scheeres, D.J., Ostro, S.J., Hudson, R.S., De Jong, E.M., Suzuki, S.: Icarus **132**, 53 (1998)
Scheeres, D.J., Williams, B.G., Miller, J.K.: J. Guid. Control Dyn. **23**, 3 (2000)
Scheeres, D.J., Durda, D.D., Geissler, P.E.: In: William, F., et al. (eds.) Asteroids III, p. 527. University of Arizona Press, Tucson (2002)
Scheeres, D.J., Gaskell, R., Abe, S., et al.: In: AIAA/AAS Astrodyn. Specialist Conf. Exhibit (Colorado), p. 21 (2006)
Szebehely, V.: Theory of Orbits: The Restricted Problem of Three Bodies. Academic Press, New York (1967)
Tricarico, P., Sykes, M.V.: Planet. Space Sci. **58**, 12 (2010)
Walsh, K.J., Richardson, D.C., Michel, P.: Nature **454**, 188 (2008)
Walsh, K.J., Richardson, D.C., Michel, P.: Icarus **220**, 514 (2012)
Werner, R.A., Scheeres, D.J.: Celest. Mech. Dyn. Astron. **65**, 313 (1997)
Yeomans, D.K., Antreasian, P.G., Barriot, J.P., et al.: Science **289**, 2085 (2000)
Yu, Y., Baoyin, H.: Astron. J. **143**, 62 (2012)